JET–P(97)28

Dedicated ITER H-mode Power Threshold Experiments with the MkI Pumped Divertor

E Righi, A Bickley, D J Campbell[1], JG Cordey, J Ehrenberg, R Giannella[3], J de Haas[2], P Harbour, N C Hawkes[4], A Howman, A Loarte[1], R D Monk, P Nielsen, L Porte[5], D F H Start, D Stork, K Thomsen.

JET Joint Undertaking, Abingdon, Oxfordshire, OX14 3EA, UK.
[1]The NET Team, Garching bei Munchen, Germany.
[2]Netherlands Foundation for Research in Astronomy, Dwingeloo, NL
[3]CEA/Euratom Association, Cadarache, France.
[4]UKAEA/Euratom Association, UKAEA Fusion, Culham, Abingdon, UK.
[5]Department of Electrical Engineering, UCLA, California.

To be submitted to Plasma
Physics and Controlled Fusion

October 1997

Abstract

In this paper the results from the first series of JET experiments dedicated to the investigation of the properties of the H-mode power threshold are presented. The experiments were carried out in an ITER-like magnetic equilibrium and made use of the Mark I Pumped Divertor. Scaling of the threshold power is investigated in terms of both global variables and local edge parameters. First evidence of the existence of a minimum edge temperature (T_{crit}) necessary for the L-H transition is reported. Deviation from the linear density scaling of the threshold power, observed at $\overline{n}_e > 5\times10^{19}$ m^{-3} (70% of the Greenwald limit at 3MA) is shown to be due to detachment and MARFE-like structures at the divertor during the L-mode phase, the effect of which is to keep the plasma edge cool and $T_e < T_{crit}$.

1. INTRODUCTION

The H-mode is a divertor plasma regime with high energy and particle confinement which was found first on tokamaks (Wagner et *al.* 1982), and more recently on stellarators (Erckmann et *al.* 1993). A necessary condition for obtaining the H-mode regime is that the power coupled to the plasma exceeds a certain threshold. The threshold power, P_{THRES}, has been found to depend on magnetic field, density, gas species of the main plasma, (ASDEX Team 1989, JFT-2M Team 1991, Ryter et *al.* 1992, Lackner et *al.* 1994), direction of the ion ∇B drift (JFT-2M Team 1991, Nardone et *al.* 1991, Ryter et *al.* 1992, Ward et *al.* 1991, Start et *al.* 1994, Lackner et *al.* 1994), wall conditioning, plasma-limiter distance (Ryter et *al.* 1996) and machine size (Ryter et *al.* 1996, Carlstrom et *al.* 1996). At present the design of the International Thermonuclear Experimental Reactor (ITER) relies on H-mode confinement to achieve ignition. It has therefore become important to establish how P_{THRES} varies especially with size, density and magnetic field so that a reliable prediction can be made of how much auxiliary heating power is required on ITER to access the H-mode regime. The ITER Threshold Database (Ryter et *al.* 1992) was assembled in an attempt to find such scalings.

In 1994 the ITER Confinement and Transport Expert Group asked Alcator C-MOD, ASDEX-U, COMPASS-D, DIII-D, JET, JFT-2M, JT60U and PBX-M to carry out a series of experiments in an ITER-like magnetic configuration (Righi et *al.* 1995).The aim of the experiment was to determine the density and magnetic field dependence of the threshold power for each device in the same geometry. This paper reports the detailed analysis of the experiments carried out on JET using the MkI Pumped Divertor, with particular emphasis on the relationship between threshold power and edge conditions.

The paper is organised as follows. In Section 2 the criteria used to select the time-points that form the database are described. In Section 3 the results of ITER dedicated experiments on JET are presented. In Section 3.1 the dependence of the power threshold P_{THRES} on the central

line averaged density is determined and compared with the latest scaling expressions from the multi-machine ITER Threshold Database (Ryter et *al.* 1996, Takizuka et *al.* 1996). Although the main aim of the experiment was to determine the scaling of P_{THRES} with density and magnetic field, a considerable effort was also put into obtaining measurements of density and temperature at the plasma edge during the L-H transition. Thus in Section 3.2 the analysis is focused on the dependence on edge density and temperature of the net power flowing through the separatrix. In Section 3.3 the results obtained in the high density regime are described. It is shown that under these conditions the plasma becomes detached at the inner divertor and in extreme cases a divertor instability appears. For these discharges an input power well above that expected with a linear density scaling is necessary to re-attach the inner divertor leg and obtain the H-mode. This conclusion is supported in Section 3.4 by neutral pressure measurements in the main chamber and in the divertor. Finally in Section 4 the results are summarised.

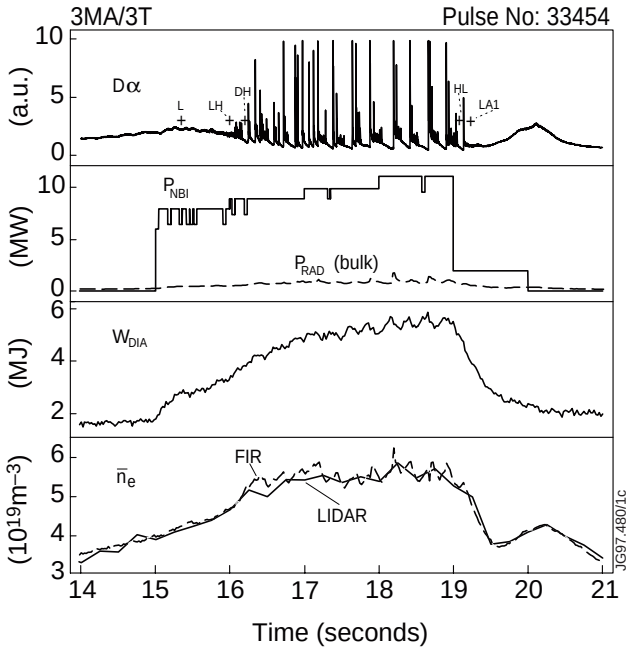

Figure 1. Example of the discharge type used in the dedicated experiments. The NBI power was increased in steps of 0.7MW (in this example) in order to minimise the uncertainty on the determination of P_{THRES} and at the same time contribute to fuelling in a controlled way. In the figure the crosses indicate the different H-mode phases and where the time-points of the Threshold Database have been taken.

2. THE THRESHOLD DATABASE

The time-points that form the database of the present analysis are labelled following the conventions of the ITER Threshold Database. Thus a steady-state L-mode time-point (at a power level for which no H-mode transition occurs) is indicated with L, while an L-mode pre-transition to a dithering H-mode is indicated by LD. An L-mode pre-transition to either an ELMy or an

ELM-free H-mode is instead labelled as LH (that is, no distinction is made between ELMy and ELM-free transition). A dithering pre-transition to an H-mode (again either ELMy or ELM-free) is indicated as DH. The time-points relative to L-H transitions have been selected about 30 msec before or after the transition itself. Apart from the slope of the diamagnetic energy (see Section 3.2 for details), all data have been obtained by averaging the signals over a ±25msec interval around the time-point. It is of vital importance to know if ITER can reach its operating point ($\overline{n}_e = 10^{20}$ m^{-3}) starting from an H-mode transition at low density and without degradation of confinement. Therefore since 1994/95 one of the aims of the ITER Threshold Database has been to collect information about the H-L transition as well, in order to establish how the H to L power threshold P_{HL} scales with the main plasma parameters. The relevant time-points are taken about 30msec before and after the H-L transition and averaged over a ±25msec, are labelled HL and LA1, respectively. The typical sequence of time-points set during an H-mode as described above is shown in Fig.1. The L-H transition is identified by the drop of the D_α signal coincident with the simultaneous increase of electron density, diamagnetic energy and energy confinement time. The transition is usually dithering, characterised by small "grassy,, ELMs (typical of the transition) and followed by a short ELM-free phase. Type I ELMs usually follow at low-medium density, while Type III ELMs are present at high density. The discharges used to form the database used in the present analysis (both L- and H-modes) have also been included in the ITER Threshold Database.

3. THE ITER DEDICATED POWER THRESHOLD EXPERIMENTS

The experiment was carried out during the MkI divertor campaign in a single null ITER-like X-point low flux expansion configuration, with divertor target tiles made of either CFC or beryllium. The main plasma was separated by about 8cm from both the inner and the outer limiters, with the X-point about 25cm above the divertor target plates (see Fig.2 for an example of magnetic equilibrium). The average triangularity was maintained at $\delta \cong 0.15$. The condition $q_{95} \cong 3$, adopted for the ITER reference scenario during the experiment, translated on JET into three feasible combinations of plasma current I_p and toroidal magnetic field B_t: 1MA/1T, 2MA/2T, 3MA/3T. In all cases the ion ∇B drift was directed towards the divertor target plates (normal/positive toroidal field direction). The auxiliary heating system used was 80 kV and 140 kV D^0 NBI in a D plasma. The NBI power was increased gradually in steps of 0.7 MW or 1 MW at a time, each step lasting for about 1 sec (Fig.1 shows a typical example). This restricts the uncertainty in the threshold power due to NBI to less than 1 MW. Moreover such a power "staircase,, could be used to control the contribution of NBI to plasma fuelling by changing the ratio of 80/140 kV beams. During the experiment divertor pumping was provided by the cryopump (Saibene et *al.* 1995).

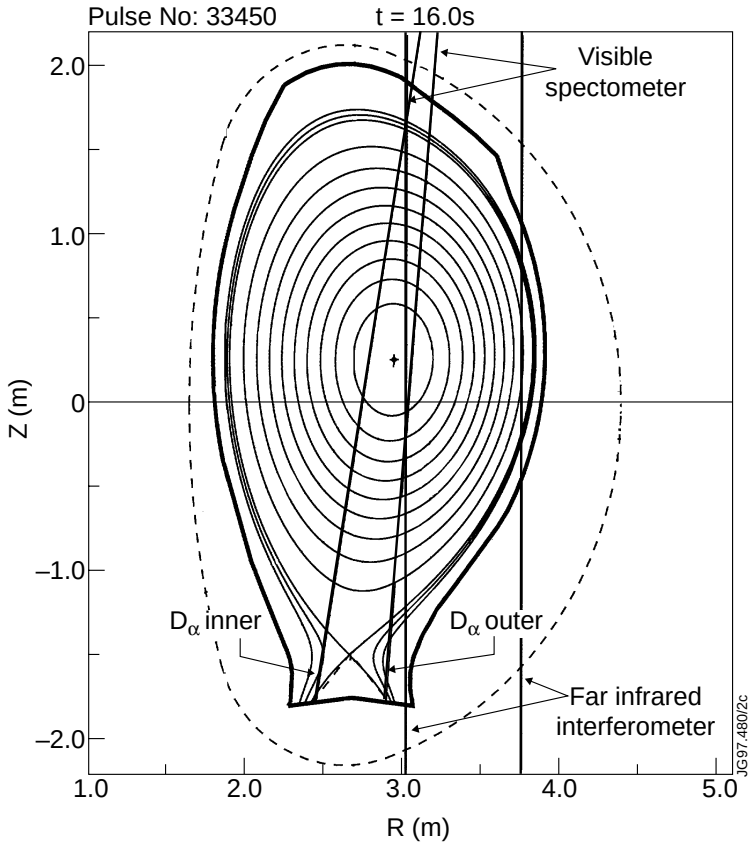

Figure 2. Example of a typical EFIT equilibrium reconstruction for the series of discharges dedicated to the investigation of the density scaling of the power threshold in JET with the MkI Pumped Divertor. Some of the lines of sight of the visible spectrometer and the far infrared interferometer are also shown. The figure corresponds to a 3MA/3T plasma.

For each I_p/B_t combination both gas puffing and controlled fuelling of NBI (through the power staircase) were used to reach the required density. The main aim of the experiment was to determine the density scaling of the H-mode power threshold. Therefore measurements of the plasma density have been carefully validated by checking the results from the Far InfraRed (FIR) interferometer against those obtained with LIDAR Thomson scattering. In Fig.3 such a validation procedure is reported for both the central line averaged density $\overline{n}_e$ (Fig.3a) and the line integrated electron density near the plasma edge, from which the edge line averaged density $\overline{n}_{ea}$ is derived (Fig.3b).

Experiments using Ion Cyclotron Resonance Frequency (ICRF) heating have unfortunately been rather limited during the Experimental Campaign with the MkI Divertor. For these discharges, also included in the 1994/95 Threshold Database, edge measurements could not be taken, and therefore will be excluded from most of the present analysis. However an extensive series of experiments using ICRF heating alone, complementary to those presented in this paper, has been carried out during the Experimental Campaign with the MkIIa Pumped Divertor, both with and without plugging of the by-pass leaks (Righi et *al*. 1997).

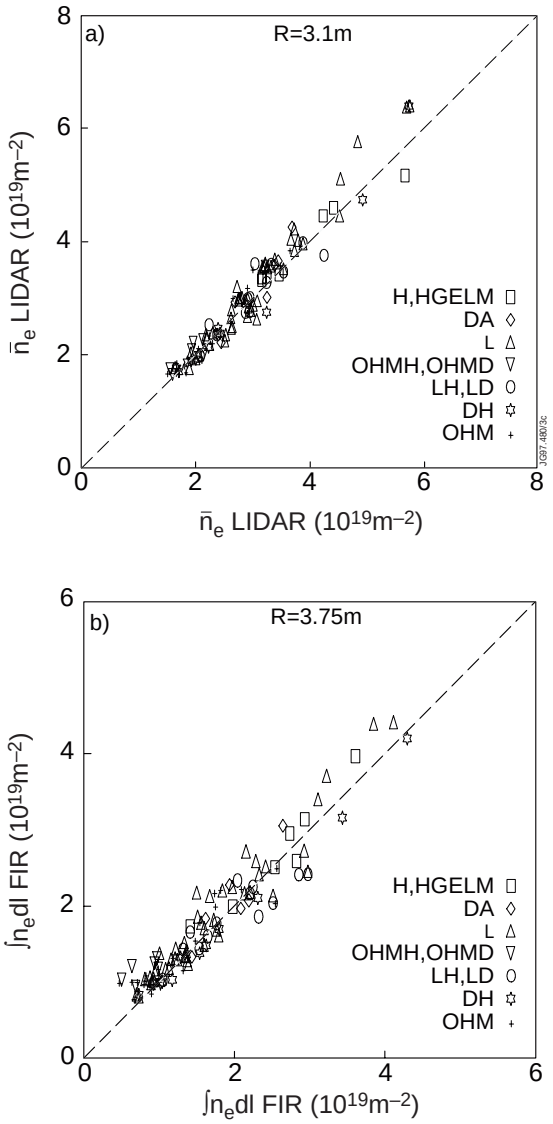

Figure 3. The electron density has been validated by checking the values obtained at the time-points indicated in the legend. with the FIR Interferometer against those from LIDAR. In Fig.3a the central (R=3.1m) line averaged density $\overline{n}_e$ is shown, while in Fig.3b the validation of the line integrated density at R=3.75m is reported. From this latter measurements the edge line averaged density $\overline{n}_{ea}$ is derived.

3.1. The Threshold Power at the Plasma Edge

A number of theories interpret the transition to H-mode essentially as a plasma edge phenomenon. It is therefore useful to characterise the threshold power at the plasma edge. This involves more and more sophistication in the estimate of P_{THRES}. When no other information is available, the power threshold for the L-H transition can be defined simply as the total power coupled to the plasma estimated at the L-H pre-transition time-points LD,LH,DH:

$$P_{THRES} = P_{TOT} \equiv (P_{OHM} + P_{AUX})_{t=LH,\,LD,DH} \ , \qquad (1)$$

where P_{OHM} is the Ohmic power dissipated into the plasma, while P_{AUX} is the power coupled to the plasma by the auxiliary heating system used (NBI in the case of the dedicated experiments considered in this paper, but also Ion Cyclotron Resonance Frequency heating for JET).

In order to identify as accurately as possible the power threshold the NBI power is corrected for possible re-ionisation losses in the beam ducts and, when possible, for shine-through losses, which become especially important at low density. On JET power losses due to ripples of the magnetic field are minimal under normal circumstances (Tubbing et *al.* 1995) and are therefore neglected in the analysis.

A further refinement in the estimate of the threshold power can be made if the rate of change dW_{DIA}/dt of the diamagnetic energy W_{DIA} is known. The role of dW_{DIA}/dt is twofold. Firstly, as in the estimate of the confinement time τ_E, the rate of change of W_{DIA} is an estimate of how much power remains confined in the plasma centre, and therefore does not flow back to the separatrix. Secondly, dW_{DIA}/dt takes into account changes in the plasma energy due for instance to the presence of a fast ion population, especially important when ICRF heating is used. Thus the threshold power can also be defined as,

$$P_{THRES} \equiv P_{LOSS} = P_{TOT} - dW_{DIA} / dt \ . \tag{2}$$

The estimate of dW_{DIA}/dt is a delicate process, since smoothing of the source signal W_{DIA} is required without losing information about the slope. A centre-averaging method has been used to smooth the raw signal from the diamagnetic loop over a ±200 msec interval, and calculates dW_{DIA}/dt with a normal accuracy of 20%. Averaging over such a wide time interval is necessary due to the presence of a 4 Hz oscillation in the diamagnetic signal, shown in Fig.4, and originating from the sweeping of the strike zones across the divertor target plates. The oscillation of W_{DIA} does not correspond to a real oscillation of the plasma during sweeping, and the only way to ensure that dW_{DIA}/dt does not give the rate of change of the oscillation, rather than the real slope of W_{DIA}, is to average over at least ±200 msec. Unfortunately such a method is not suited to study fast transients. However, as shown in Fig.4, the calculation is adequate for pre-transition L-mode time-points.

The definition of threshold power can be taken one step further to include radiation losses. Here P_{THRES} is defined by the power balance at the separatrix,

$$P_{THRES} \equiv P_{NET} = P_{TOT} - dW_{DIA} / dt - P_{RAD}^{bulk} \ , \tag{3}$$

or equivalently the power density flux across the separatrix,

$$Q_{SEP} \equiv (P_{TOT} - dW_{DIA} / dt - P_{RAD}^{bulk}) / S , \tag{4}$$

where P_{RAD}^{bulk} is the power radiated by the bulk plasma, measured with a multiple line-of-sight ex-vessel bolometer, and having a 10% accuracy. The surface area S of the plasma is estimated through a full magnetic equilibrium calculation (EFIT), which in JET is provided by the

reconstruction of the plasma boundary based on the measurements of the magnetic pick-up loops. The accuracy of the surface area data is estimated to be 5%. It is thus clear that in the estimate of the threshold power at the plasma edge the biggest source of uncertainty comes from the estimate of dW_{DIA}/dt.

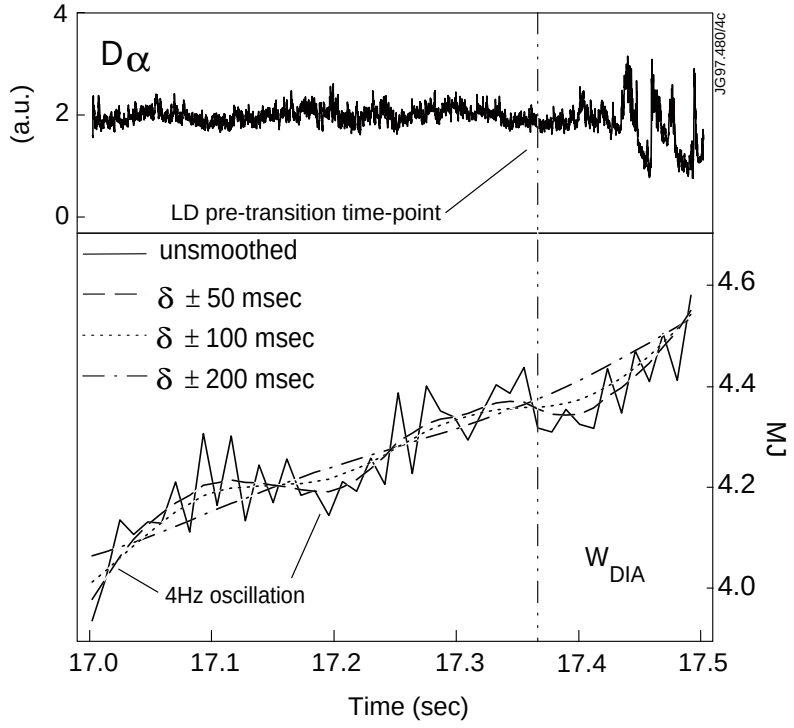

Figure 4. The diamagnetic energy signal W_{DIA} shows a spurious 4Hz modulation originating from the sweeping of the strike zones on the divertor target tiles and picked up by the diamagnetic loop. In order to determine the slope of W_{DIA} it is therefore necessary to smooth the signal over a ±200 msec interval. In the figure the result of smoothing the signal with different intervals around a L-H pre-transition time-point is shown.

3.2 Scaling of the Threshold Power with Global Plasma Variables

As shown in the previous Section, refinement of the definition of threshold power in terms of balance at the plasma separatrix involves the introduction of large uncertainties, mostly related to the estimate of dW_{DIA}/dt. In view of this, and of the difficulty in some cases to obtain sufficiently accurate estimates of dW_{DIA}/dt, it is convenient to display the power threshold data by using in the first instance the definition given by Eq.(1), that is in terms of the total coupled power needed to obtain the transition to H-mode. The threshold power can thus be validated for each I_p/B_t combination by comparing the data-points representing the L-H transitions (LD,LH,DH), selected using the criteria discussed in Section 2, against the database formed by steady-state L-mode points (L). The threshold power is then identified as the lowest power for which the H-mode can be formed for a given set of plasma conditions. An example of such an existence diagram is shown in Fig.5 for the 3MA/3T series of data.

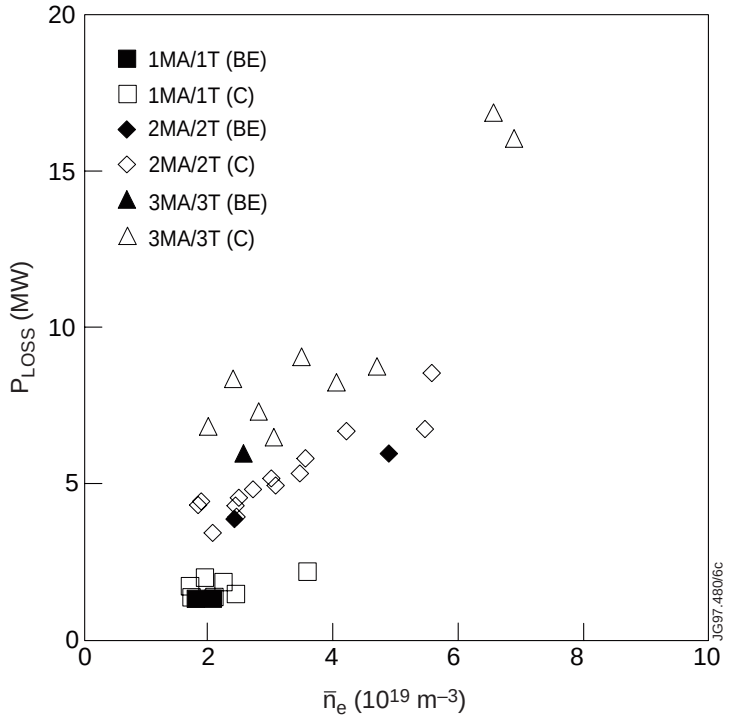

Figure 5. The power threshold is determined by establishing the dividing line between L-H pre-transition points and steady-state L-mode points obtained from plasmas which did not enter the H-mode. This figure shows an example for the series of data obtained at 3MA/3T. Although L-H pre-transition points between 5 and 7×10^{19} m^{-3} are absent, the trend of the steady L-mode points confirms the deviation from linearity discussed in the text.

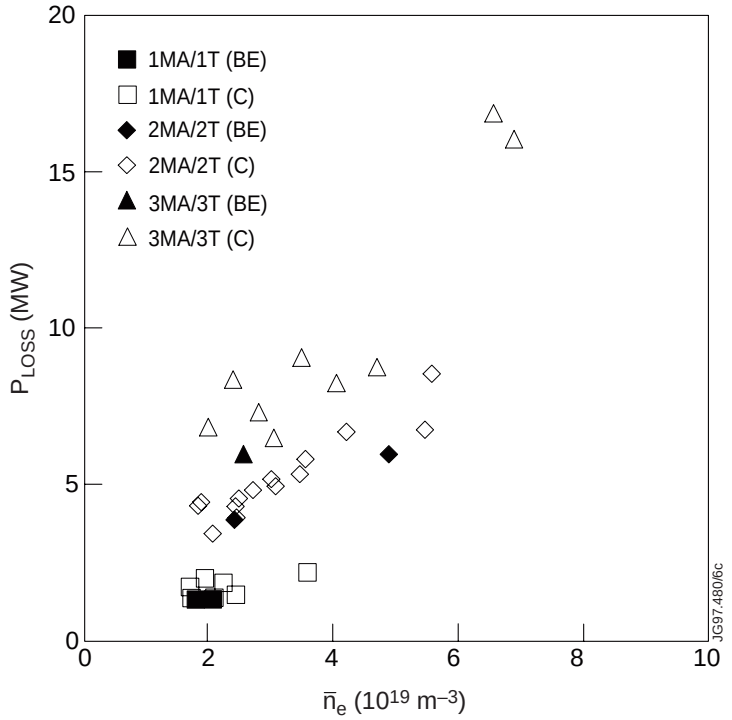

Figure 6. After the power threshold has been validated for all I_p/B_t combinations of the experiments, the results are combined to give as overall impression. The solid symbols indicate the L-H transitions obtained with beryllium divertor target tiles, the open symbols those with CFC tiles.

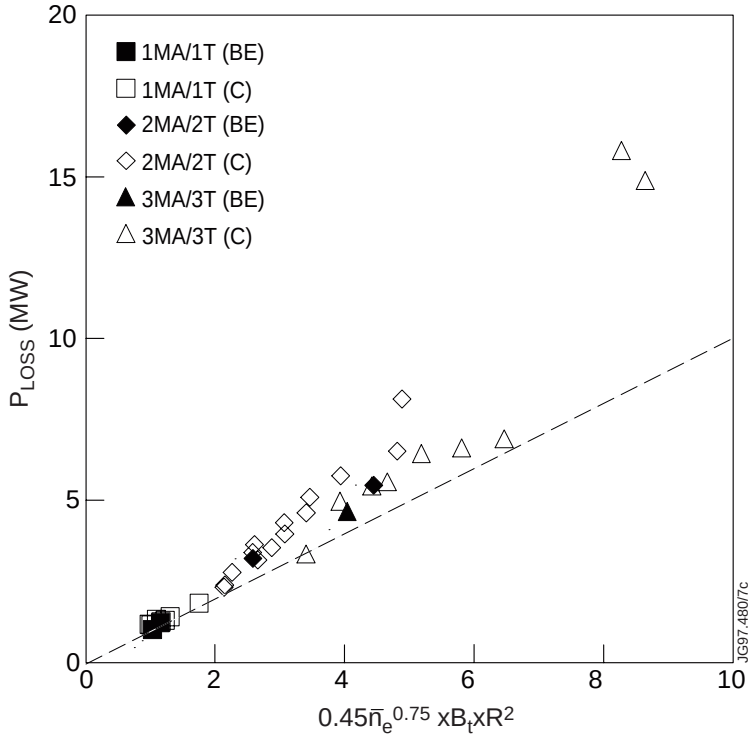

Figure 7. The experimental threshold data agree well with the multi-machine scaling expression given by Takizuka et *al*. (1996).

The dependence of P_{THRES} on the central line averaged plasma density $\overline{n}_e$ is summarised in Fig.6 for each of the I_p/B_t combinations investigated in JET. Although P_{THRES} scales approximately linearly with $\overline{n}_e$, deviations from the linear scaling are evident both at high and low densities, especially in the 3MA/3T series. In fact, as discussed in detail in Section 3.4, the high density discharges at 3MA/3T and 2MA/2T provide important information about the transition into H-mode and H-mode behaviour in high density target plasmas. Once the total coupled power used to obtain the H-mode transition has been validated through the procedure outlined in Fig.5, the data can be compared with the most recent dimensionally correct scaling expression for ITER (Takizuka et *al*. 1996),

$$P_{THRES} = P_{TOT} - dW_{DIA} / dt = 0.45 \times \overline{n}_e^{0.75} \times B_t \times R^2 \ , \qquad (5)$$

where R is the plasma geometrical major radius in metres and the other quantities have been introduced earlier. Comparison of the data with Eq.(5) is shown in Fig.7, where the threshold data fit the scaling expression reasonably well at low and moderate densities, but deviations from the fitting are again evident at high values of the abscissa for both the 2MA/2T and 3MA/3T discharges. There are however other scaling expressions, equally valid, which have a different dependence on geometry (Ryter et *al*. 1996). Thus for example a dependence on the surface area such as,

$$P_{THRES} = P_{TOT} - dW_{DIA} / dt = 0.025 \times \overline{n}_e \times B_t \times S \ , \qquad (6)$$

has also been compared to JET data in Fig.8, whilst a strong R dependence is given by,

$$P_{THRES} = P_{TOT} - dW_{DIA} / dt = 0.3 \times \overline{n}_e \times B_t \times R^{2.5} \ . \qquad (7)$$

It is an indication of the degree of the scatter in the multi-machine threshold database that the scalings given by Eq.(5,6,7) are equivalent, and that therefore size and density dependence cannot be at present unequivocally determined. As far as JET data considered in this paper are concerned, it can be concluded with a fair degree of confidence that the scaling given by Eq.(6) largely underestimates the power needed to obtain the H-mode. Both scaling expressions based on the radius R and given by Eq.(5) and Eq.(7) instead describe JET data reasonably well. The reason for this is that since the 1991/92 Experimental Campaign the surface area of JET plasmas has decreased by about 30% due to the introduction of the pumped divertor, while the major radius is substantially unchanged.

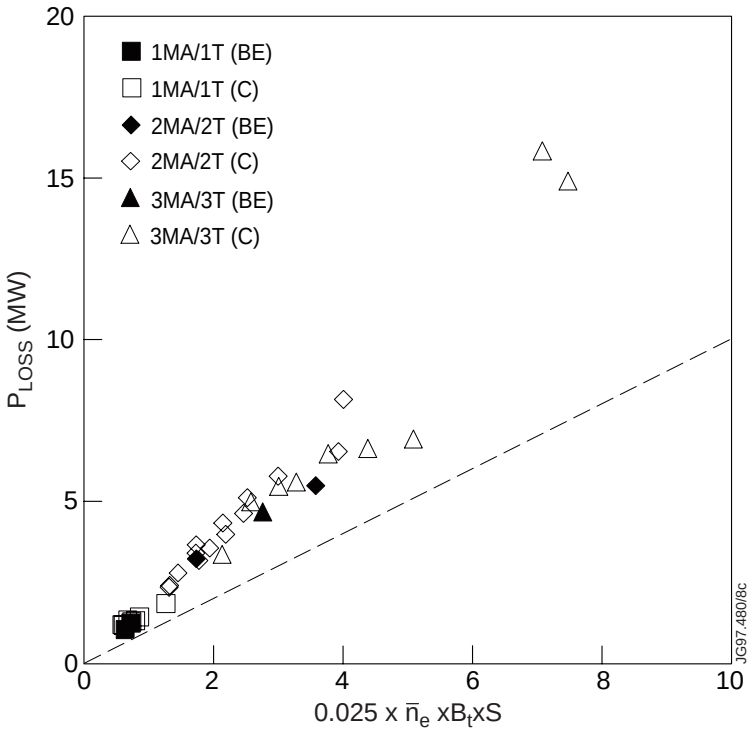

Figure 8. Scaling of the threshold power with the surface area S (Ryter et *al*. 1995) does not fit the experimental data so well as the scaling with the radius R. The reason for this is that the surface area scaling has been derived by using JET data obtained before the installation of the Pumped Divertor. As a consequence, JET plasmas have a surface area reduced by about 30% without any appreciable changes in the major radius R.

The scaling of Eq.(5) can be used to compare the power needed to obtain the H-mode with the two additional heating systems used in JET, namely ICRF heating and NBI. Such a comparison

is shown in Fig.9. In general the ICRF threshold points are lower than those obtained with NBI. This is simply due to the fact that in general ICRF power can be delivered with better accuracy, for instance by means of slow power ramps, while NBI staircases are necessarily discrete. Under similar conditions, the H-mode is obtained with similar levels of either ICRF or NBI. In this respect these two heating systems are equivalent.

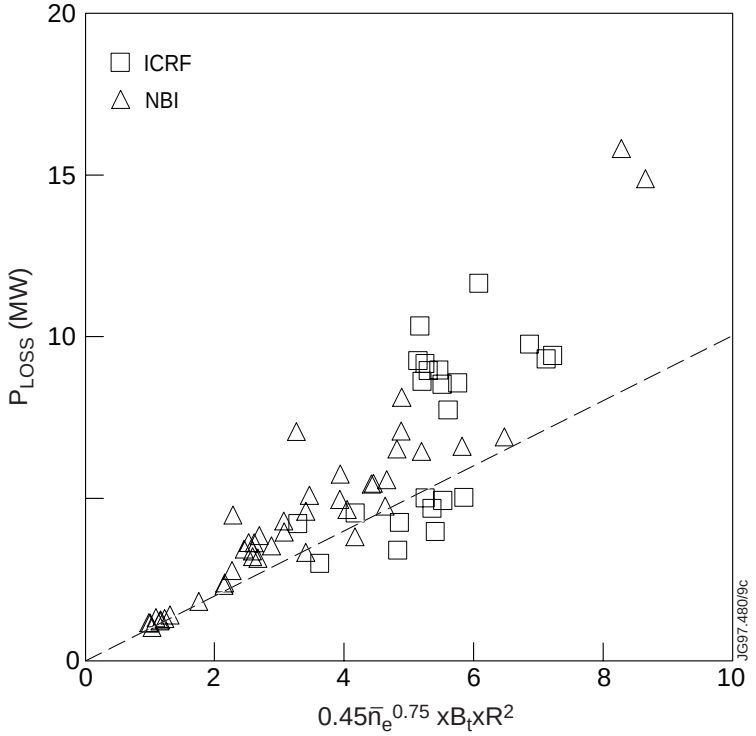

Figure 9. The threshold powers obtained with ICRF heating or NBI are comparable. The ICRF points are in general lower because better accuracy can be achieved. Note that at high values of P_{LOSS} and $\overline{n}_e$ the ICRF points also deviate from the scaling.

The main power threshold experiment was carried out with CFC divertor target tiles. However after the installation of Be target tiles a number of selected discharges has been repeated for comparison, also shown in Fig.6. In both cases Be evaporations were carried out. Although no data at high $\overline{n}_e$ could be obtained with Be tiles, no significant differences in P_{THRES} could be found with different target tile materials. From this we must conclude that, as far as low Z materials are concerned, the composition of the divertor target tiles does not affect the power threshold.

3.3 Edge Measurements

In this series of experiments measurements at the plasma edge were obtained of quantities thought to be important for the understanding of the physics of the H-mode transition, such as

the electron density, the electron and ion temperatures and the neutral pressure at the midplane and in the sub-divertor region. In this Section the edge quantities obtained during the experiment are introduced and their relationship with the threshold power is explored.

As in the case of $\overline{n}_e$, the line averaged electron density at the plasma edge has been obtained by measuring the line integrated density with the FIR interferometer at the fixed chord R=3.75m (for the position refer to Fig.2) and subsequently divided by the chord length, taken from the equilibrium reconstruction. By comparison, the separatrix position, as estimated by EFIT reconstruction of the magnetic equilibrium, is R_{SEP}=3.82±0.02 m. The uncertainty in the FIR data is normally 5%. These measurements have been cross-checked against their corresponding values from LIDAR (see Fig.3b) to give a reliable estimate of $\overline{n}_e$ at the plasma edge, $\overline{n}_{ea}$.

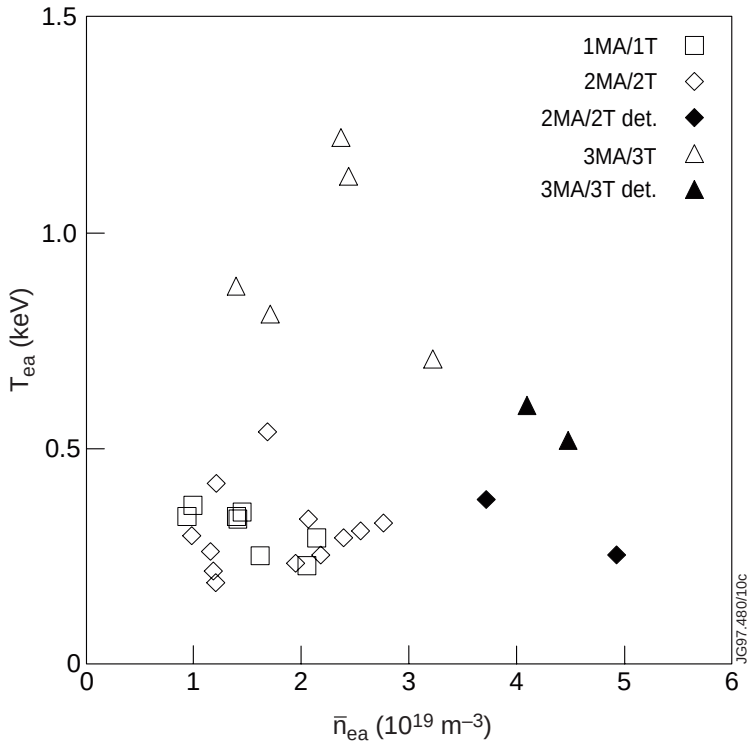

Figure 10. The edge electron temperature T_{ea}, measured at R=3.75m with the Michelson interferometer and cross-checked with the heterodyne radiometer, shows very little dependence on the edge density, but a rather strong scaling with the toroidal field B_t. The solid symbols in the figure refer to discharges where the inner divertor leg is partially or completely detached.

The measurement of the electron and ion temperatures at the edge have been more difficult to obtain. The edge electron temperature T_{ea} was been measured with the ECE Michelson interferometer for B_t values of 2T and 3T and cross-checked against the heterodyne radiometer for B_t=2T, for which high resolution measurements exist. The estimated error on the edge temperature is 12%, due mainly to poorer resolution at the plasma edge than in the core (for which the error is usually 5%). Due to technical limitations intrinsic to the ECE diagnostics, no

measurements exist for the 1T discharges. There are measurements from LIDAR Thomson scattering, but with a larger uncertainty due to the poor spatial resolution at the edge (about 5cm). The set of measurements thus obtained are shown in Fig.10, from which it can qualitatively be concluded that T_{ea} depends weakly on the edge density. The magnetic field dependence is less clear, although it seems quite strong (more than linearly). In particular the large scatter in the 3MA/3T data is not understood. Such results have been confirmed recently also by other machines, like Alcator C-MOD (Snipes et *al.* 1996), DIII-D (Groebner et *al*. 1996) and ASDEX-U (Kaufman et *al*. 1996).

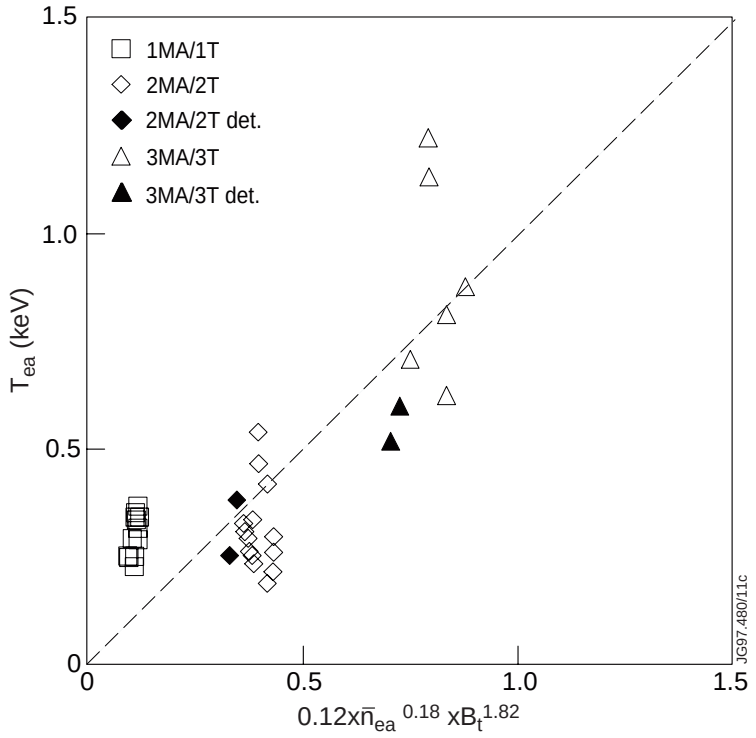

Figure 11. Regression analysis on the data quantifies the qualitative scaling of Fig.10: the spread of the data around the calculated values reflects the uncertainty in the data.

Recently it has been suggested that the L-H transition could be determined by edge conditions linked to the edge electron pressure (Groebner et *al.* 1996). In particular, the H-mode transition would occur when a maximum value of the plasma β is reached, for which large-scale turbulence is suppressed. Such a condition on β would translate into a condition on the edge density and temperature and the magnetic field of the type $\bar{n}_{ea} T_{ea} / B_t^2 \approx \text{const}$. Indications of how T_{ea} at the L-H transition, T_{crit}, could depend on the magnetic field and edge density can be obtained by a least-squares fit to the experimental data with an expression of the form $T_{ea} = a \times \bar{n}_{ea}^{a1} \times B_t^{a2}$. Any dependence on edge geometrical quantities, like surface area, elongation or major radius, is not included in the scaling since for these experiments they were kept fixed. The result confirms the scaling suggested by Fig.10,

$$T_{crit} = (0.09 \pm 0.05) \times \bar{n}_{ea}^{(-0.08 \pm 0.15)} \times B_t^{(1.97 \pm 0.47)} \quad . \tag{8}$$

The quadratic dependence on B_t is well represented by the regression analysis, but Eq.(8) implies a rather weak dependence on the edge density. Fig.10 and Eq.(8) have been derived by deliberately including also all those discharges which show anomalous behaviour at the divertor, and as a consequence need more power for the L-H transition than the scaling of P_{THRES} with $\bar{n}_e$ and B_t predicts (see Sections 3.4 and 3.5). Since the scaling of Eq.(8) is valid for these discharges as well, we can conclude that, for those discharges where divertor anomalies are observed at high density, more power is needed to reach the edge temperature necessary for the H-mode transition than normally necessary.

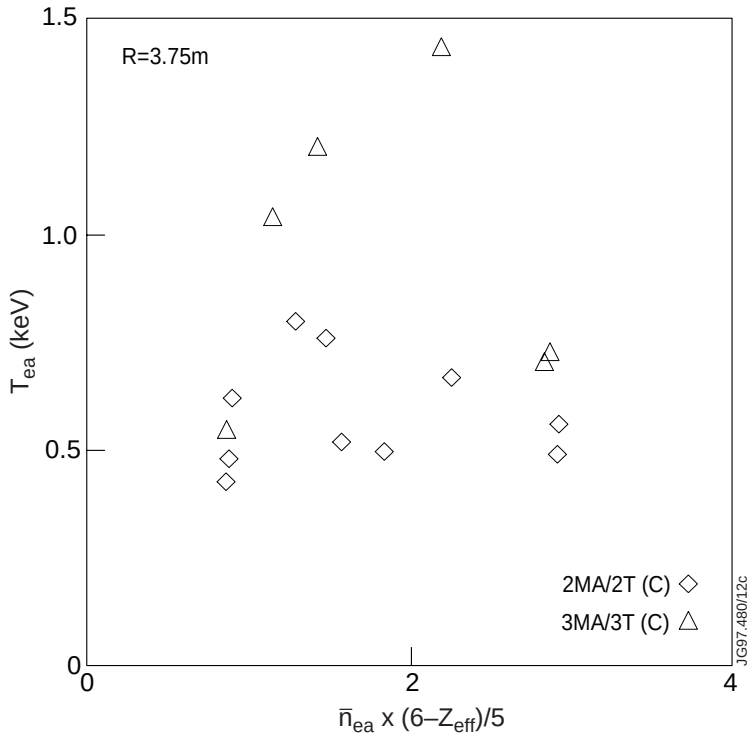

Figure 12. Measurements of T_i at R=3.75m have been taken with the Charge Exchange Recombination Spectroscopy diagnostic. The edge ion density has been estimated from the edge electron density $\bar{n}_{ea}$ and the plasma Z_{eff}, assuming Carbon as the main plasma impurity. Although less data are available than for T_{ea}, the same pattern arises, with little dependence on the density. Data at 1T are not shown because Z_{eff} is not available.

The uncertainty in the threshold temperature for the L-H transition is given by the spread of the data around the fitting line, as shown in Fig.11. The biggest source of uncertainty is in the density scaling. Information on the critical temperature determined by Eq.(8) will be used in Section 3.4, where the high density regime is discussed. As Snipes et *al.* (1996) have suggested, Eq.(8) is a necessary condition for the L-H transition. However there are not enough data to establish if this condition is also sufficient.

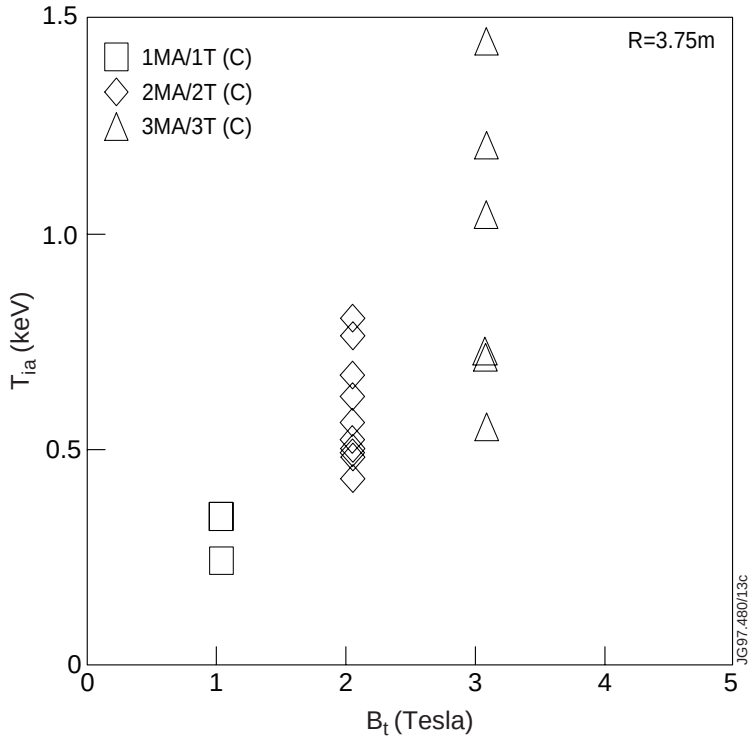

Figure 13. The edge ion temperature T_{ia} scales linearly with the magnetic field B_t.

The edge ion temperature T_{ia} has also been measured (at R=3.75m) by the charge-exchange spectroscopy diagnostics. Although the uncertainty on T_{ia} is greater than that on T_{ea} and there are fewer measurements available, the same pattern emerges qualitatively, with a weak dependence on the edge density (Fig.12) but linear scaling with B_t (Fig.13).

3.3.1 Scaling of the Power Threshold with Edge Parameters

It is reasonable to assume that in large machines the fraction of the input power lost through radiation is less than that of small machines. Nevertheless when available radiation losses should be included in the analysis if edge parameters are used to determine the scaling of the power threshold. For this reason the power threshold may be taken to be that more generally defined by Eq.(3), i.e. the net power flowing through the separatrix immediately before the L-H transition. The advantage of using an expression like P_{NET} should be evident in all those cases where an apparent increase of the power needed to obtain the H-mode can be explained by excess radiation cooling the plasma edge. Of course it is uncertain as to what fraction of the total radiated power should be used to evaluate P_{NET}. Since it is difficult to determine how much radiation is actually inside the separatrix, especially near the X-point. Eq.(3) uses the power radiated by the bulk plasma based on the assumption that the power flowing through the separatrix is the key parameter. However, it should be stressed that radiative cooling from the edge regions outside the separatrix

(the scrape-off layer, or the divertor) could heavily influence the formation (and subsequent evolution) of the H-mode. This could be all the more important for the radiative divertor scenarios envisaged for ITER.

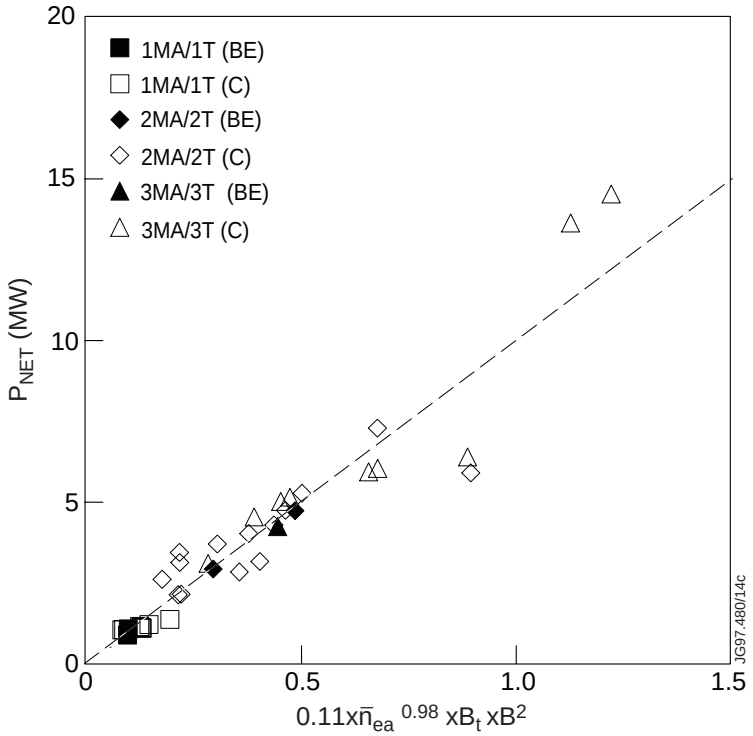

Figure 14. A scaling law that depends on edge quantities has been derived and compared to the data. A more general definition of the threshold power at the plasma edge is given by the power balance through the separatrix, P_{NET}, calculated by taking into account also radiation losses from the bulk plasma. The deviation from the linear density scaling is much less evident at the edge, but still present.

Scaling expressions equivalent to those given by Eq.(3) can be obtained by considering the edge density $\overline{n}_{ea}$ and B_t. Again, since for these experiments there are no significant variations of the relevant geometrical quantities, the variable R is assumed to scale like in Eq.(5). Also, the linear dependence of the power threshold on the magnetic field will be kept fixed, as it seems to be the most robust scaling for all the machines contributing to the Threshold Database. A non-linear regression analysis of the data can thus be carried out to determine the scaling of the threshold power at the plasma edge with the local density by assuming a model like $P_{NET} = c \times \overline{n}_{ea}^{c1} \times B_t \times R^2$. The result of the regression analysis is summarised in Fig.14, where the data are shown to closely follow the expression,

$$P_{NET} = (0.12 \pm 0.01) \times \overline{n}_{ea}^{(0.95 \pm 0.09)} \times B_t \times R^2 \ . \qquad (9)$$

When radiation losses are negligible, as in the case of this experiment, P_{NET} and P_{LOSS} should be comparable. In fact for the same dataset,

$$P_{LOSS} = (0.13 \pm 0.02) \times \bar{n}_{ea}^{(0.95\pm0.09)} \times B_t \times R^2 \ , \qquad (10)$$

which, within the error given by the asymptotic standard error, coincides with Eq.(9).

3.4 The L-H Transition in the High Density Regime

In order to extend as much as possible the $\bar{n}_e \times B_t$ range in the JET Threshold Database a number of discharges were carried out at very high density both at 2MA/2T and 3MA/3T ($\bar{n}_e > 5\times10^{19}$ m^{-3} at the transition for 3T, corresponding to about 70% of the Greenwald limit). Unfortunately, lack of experimental time prevented us from doing the same at 1MA/1T. In Section 3.2 it was already noted that especially for the 3MA/3T series, the threshold power deviates substantially from the usual linear or near-linear density scaling that holds at lower densities. In this Section an explanation is offered for such anomalous behaviour.

The evolution of the main plasma parameters for the high density discharges is shown in Figs.15-19. In these figures the inner and outer vertical D_α signals are shown together with the ion saturation currents from the divertor Langmuir probes (Monk 1996). Several blow-ups of the interesting regions are also reported.

Of the high density discharges obtained at 2MA/2T, #33446 (Fig.15) has the lowest $\bar{n}_e$ at the L-H transition ($\bar{n}_e = 4.6\times10^{19}$ m^{-3}). From this plot it can be seen that that the divertor ion flux increases with the main plasma density, indicating that the divertor is not detached. Note that the 4Hz modulation of the ion flux is due to sweeping of the strike zones across the target plates. In contrast, #33447 (Fig.16) exhibits a typical feature of high density auxiliary heated L-mode plasmas, known as "divertor oscillations,, (Monk et *al*. 1995). These oscillations, shown in more detail in the close-up of Fig.16, are characterised by periods of low ion fluxes measured by the Langmuir probes at both the inner and outer divertor regions, followed by sharp peaks with a repetition rate of about 10 Hz. At the same time the outer D_α signal increases while the inner D_α signal decreases. Such activity may be mistakenly interpreted as ELMs, but it has been observed well below the H-mode threshold in separate experiments (Monk et *al*. 1995). Observation of this phenomenon over a wide range of discharges in the JET MkI divertor has shown that these oscillations generally appear when the main plasma density is in the region of 4-6$\times10^{19}$ m^{-3} and with P_{NBI}>3.5 MW (Loarte et *al*. 1997). In fact at about 17.7 sec, when $\bar{n}_e \cong 4.6\times10^{19}$ m^{-3}, the divertor oscillations cease and the plasma enters the H-mode (Fig.16). Such oscillations are not limited to the divertor region, but they affect the bulk plasma too, as shown by the synchronous oscillations of line integrated density signals both near the centre and at the plasma edge (from which $\bar{n}_e$ and $\bar{n}_{ea}$ are derived). The 2MA/2T discharge with the highest threshold density (#33450 shown in Fig.17, with $\bar{n}_e \cong 5.6\times10^{19}$ m^{-3}) has all the previous features mixed together, which produces a very complicated behaviour which is the origin of the delay in obtaining the L-H

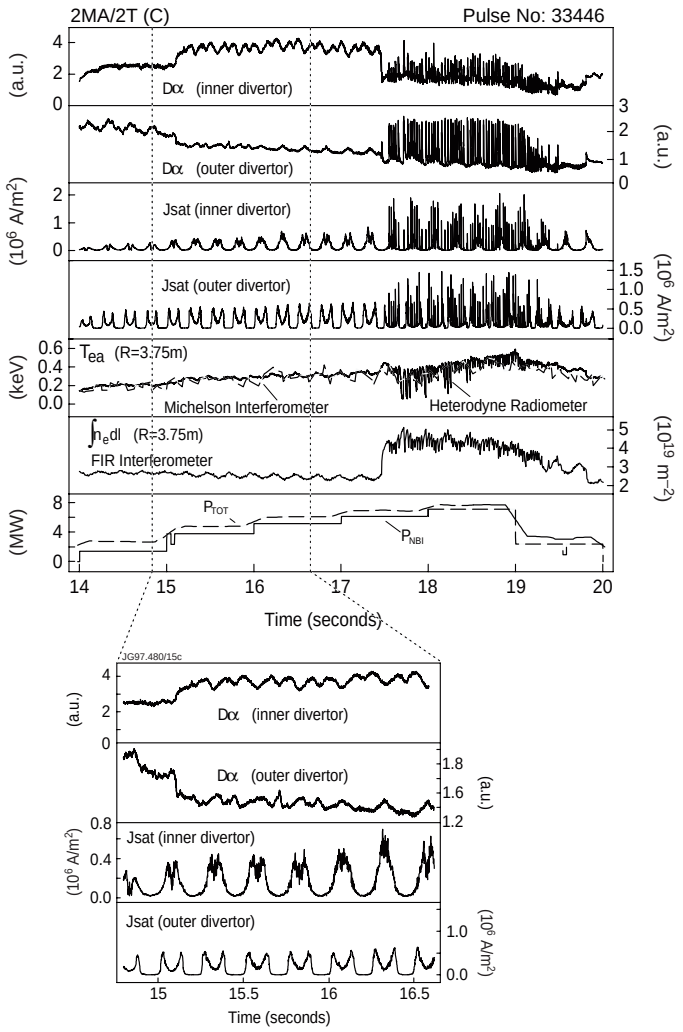

Figure 15. Time evolution of the main plasma parameters and of the signals needed to identify detachment/ oscillations in the divertor for #33446. This is the 2MA/2T discharge with lowest $\overline{n}_e$ at the L-H transition to show signs of partial detachment. The outer and inner divertor legs are monitored by the inner and outer D_α signals, and by the saturation currents of two Langmuir probes embedded in the inner and outer divertor targets. During the discharge (as in those shown in Figs. 16-19) the strike zones are swept over the divertor target at 4Hz. The electron temperature at R=3.75m is measured with both the Michelson interferometer (labelled KK1 in the picture) and the heterodyne radiometer (KK3). $T_{crit} \approx 350$ eV in this case. Other traces are the central line averaged density $\overline{n}_e$, the H89 factor and the input power. The close-up shows in more detail the behaviour of the inner and outer divertor legs, with lower J_{sat} and larger D_α for the inner divertor, typical of detachment.

transition. In fact up to 16 sec into the discharge the divertor oscillations dominate, but between 16sec and 17.3sec (time of the L-H transition) there is a mixture of divertor oscillations and "grassy,, (dithering) ELMs. After 17.3sec the conditions to maintain a clean H-mode prevail. This phenomenon can be explained in terms of the divertor physics associated with both detachment and the divertor oscillations, with reference to the close-ups of Fig.17. At the onset of the oscillations the plasma is detached from both divertor legs, the majority of the radiation

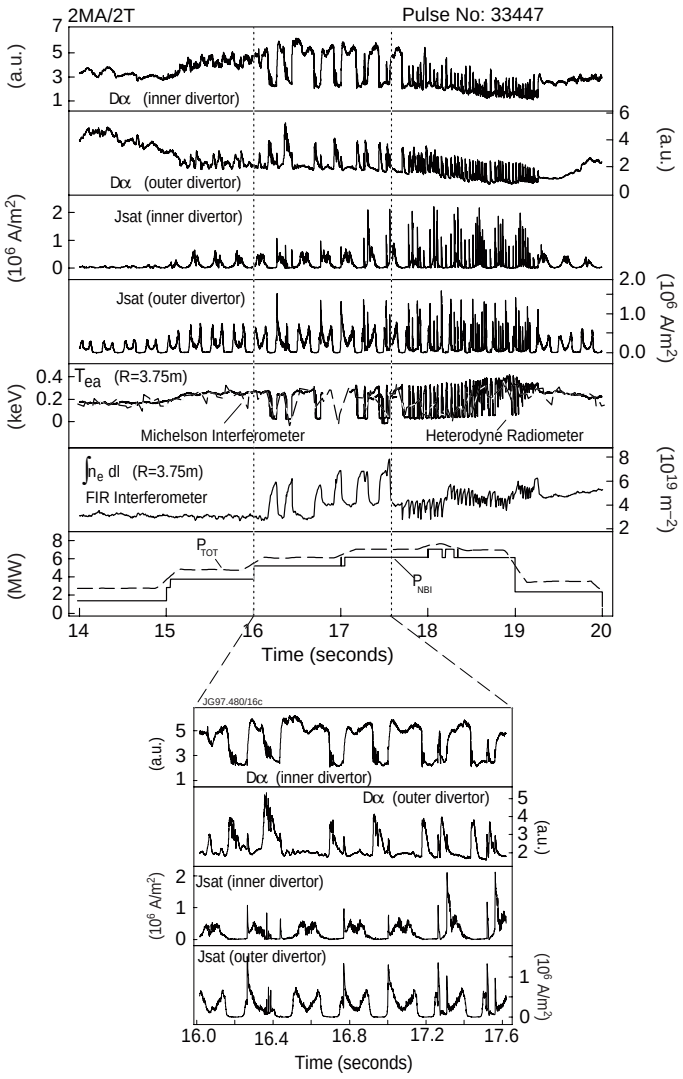

Figure 16. The same parameters of Fig.15 are here shown for #33447, another 2MA/2T discharge with a density at the L-H transition higher than that of Fig.15. This discharge shows signs of oscillations in the divertor starting at about 16 sec, and shown more clearly in the close-up: the outer D_α increases as in ELM-like activity, while at the same time the inner D_α decreases. Both inner and outer saturation currents are characterised by synchronised periods of low ion fluxes followed by sharp peaks, with a repetition rate usually of 10 Hz. The oscillations disappear when the density is further increased.

moves rapidly away from the strike zones and up to the X-point region, while the bulk radiation remains at about 10-20% of the total input power. At the same time a very cold and dense plasma region appears near the X-point, with all the characteristics of a MARFE (Loarte et *al*. 1997). In the case of #33450, the simultaneous increase of both density and NBI power means that between 16sec and 17.3sec there is insufficient power to force the MARFE back to the divertor and reattach the plasma, during which time the presence of "grassy,, ELMs indicates that without detachment the plasma would be in H-mode. However the power and density range are not sufficiently high to overcome the detachment and the divertor oscillations last until 17.3sec, after which the L-H transition occurs.

The two high density discharges at 3MA/3T (#33460 in Fig.18 and #33462 in Fig.19) show a similar behaviour. In this case there are no divertor oscillations, although there is evidence for partial detachment, and until the power is increased sufficiently to "re-attach,, it (a task made more difficult by the simultaneous density increase, which instead favours detachment) the plasma remains in L-mode.

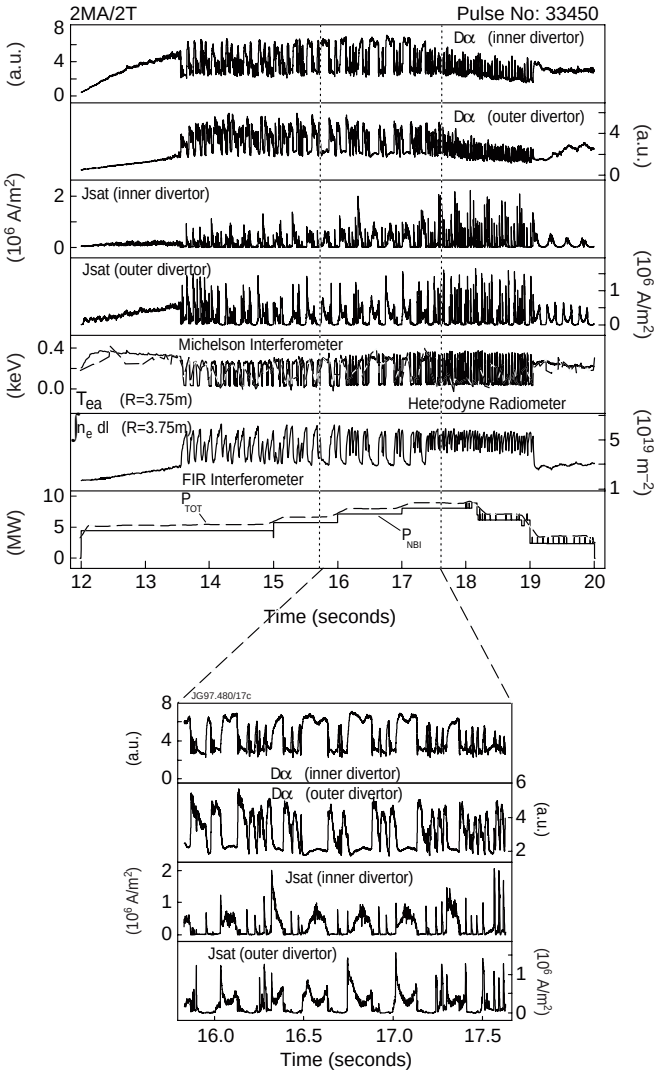

Figure 17. #33450 is the 2MA/2T discharge with the highest density at the L-H transition ($\overline{n}_e \cong 5.6 \times 10^{19}$ m^{-3}) and is characterised by a mixture of the features shown in Figs.16-17. The two close-ups show that while at first divertor oscillations dominate, between 16 sec and 17.3 sec, there is a mixture of oscillations and proper type III ELMs. After 17.3 sec the H-mode transition occurs.

Edge measurements further strengthen this interpretation for the discharges described above. The first one is the de-coupling of main chamber pressure, p_{MAIN}, from the edge density, typical of detached plasmas in which the neutral compression is reduced. This feature will be analysed

in detail in the next section. The second is the measurement of the electron temperature near the separatrix, also shown in Figs.15-19.

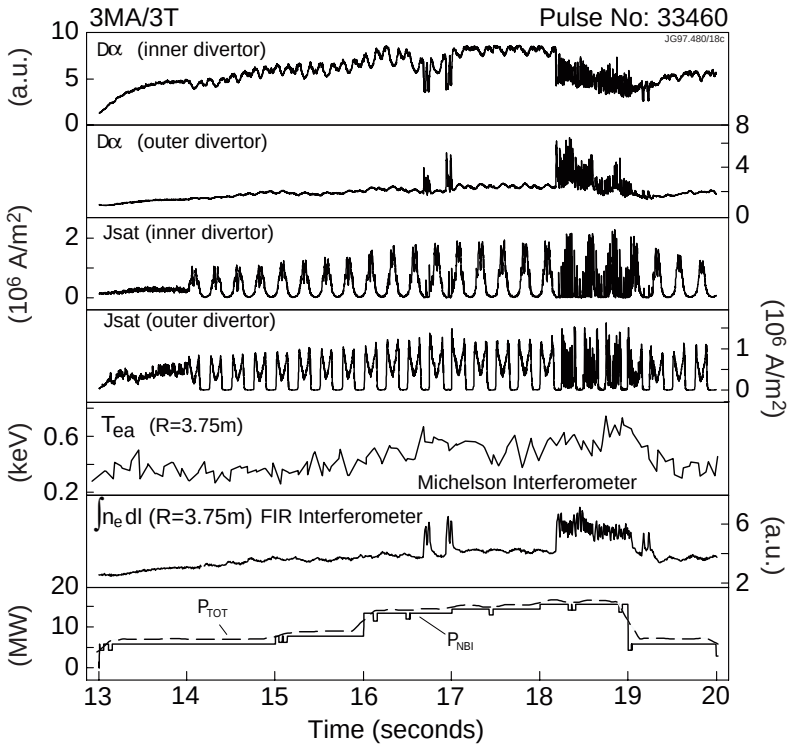

Figure 19. The 3MA/3T discharge with highest density at the L-H transition (#33462, with $\overline{n}_e \cong 7 \times 10^{19}$ m^{-3}) again remains in L-mode until detachment is overcome by power increase. Note that for this and the previous discharges $T_{ea} < T_{crit}$ (≈750 eV for B_t=3T) during the partially detached phase of the discharge.

For all the discharges it is evident that until $T_{ea} \approx T_{crit}$ (0.3-0.4 keV for 2T and 1.1 keV for 3T at R=3.75m), the L-H transition does not occur. Detachment, divertor oscillations and MARFEs are all phenomena that dissipate power at the plasma edge and are therefore deleterious for the formation of the edge transport barrier. In fact during the movement of the MARFE-like structure to the X-point region it is observed that the T_{ea} profile measured by ECE is eroded, with the formation of a hollow n_e profile. From the time evolution of T_{ea} in Figs.15-19 another important observation is that the plasma remains in H-mode as long as $T_{ea} > T_{crit}$, while Type III ELMs and the H-L transition occur when the edge temperature falls below this value. It is therefore reasonable to conclude that as far as the critical edge parameters are concerned, there is no hysteresis of the H-L transition. Results from Alcator C-MOD also support this interpretation (Snipes et *al*. 1996).

3.5 The Role of the Neutral Pressure in the H-mode Transition

The presence of neutrals has long been suspected to play a role in the H-mode transition and the overall quality of the H-mode. A difference in the H-mode confinement, linked to different recycling levels and neutral pressures, has been observed in JET with and without active pumping (Saibene et *al*. 1996).

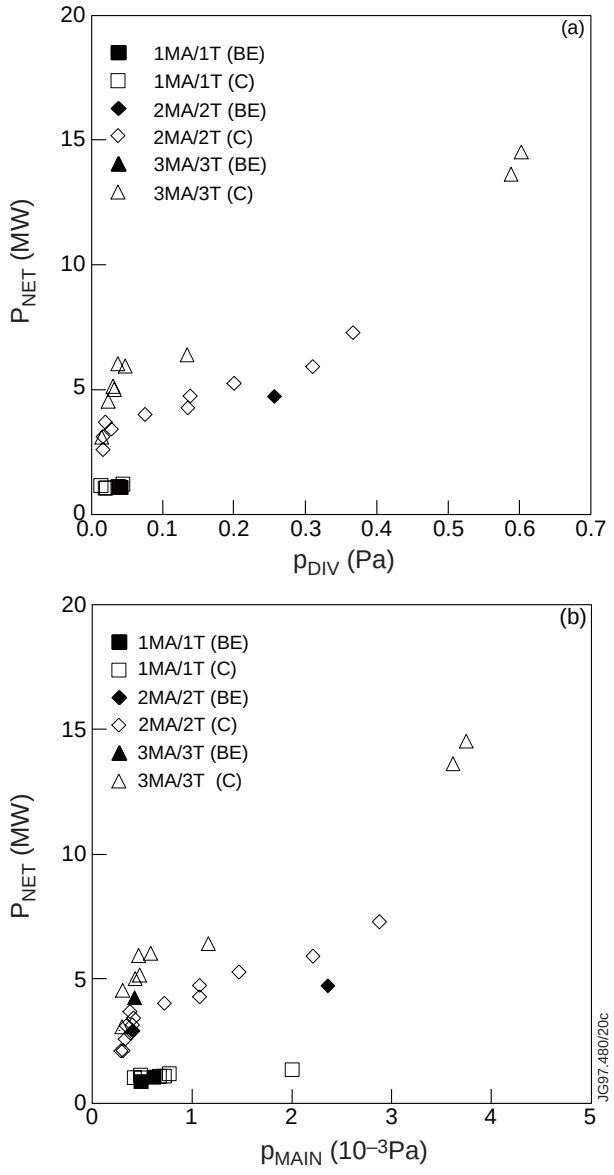

Figure 20. Dependence of the net power flowing through the separatrix P_{NET} on the neutral pressure measured by ionisation gauges near the cryopump in the sub-divertor region (Fig.20a) and at the midplane (Fig.20b). From these data there is no way to establish whether this is a real pressure dependence or if it reflects a hidden density scaling. In these experiments p_{MAIN} and p_{DIV} are closely coupled together, and their behaviour cannot be separated from that of $\overline{n}_{ea}$.

During the dedicated H-mode power threshold experiments discussed in this paper measurements of the neutral pressure both in the main chamber (p_{MAIN}) and in the sub-divertor region (p_{DIV}) have been obtained in a first attempt to understand the role of edge conditions on the L-H transition. Interpretation of these measurements has however proved to be difficult, since any pressure changes both in the divertor and in the main chamber are naturally linked to density changes near the separatrix and to the fuelling scenario. DIII-D has attempted to decouple the density scaling of the power threshold from any possible effects due to neutral pressure, but with no conclusive results (Groebner et *al*. 1996). Thus when P_{NET} is plotted as a function of the neutral pressure, like in Fig.20, it is unclear as to whether the dependence of P_{NET} on the pressure is real or it reflects a hidden dependence of p_{MAIN} and p_{DIV} on $\overline{n}_{ea}$.

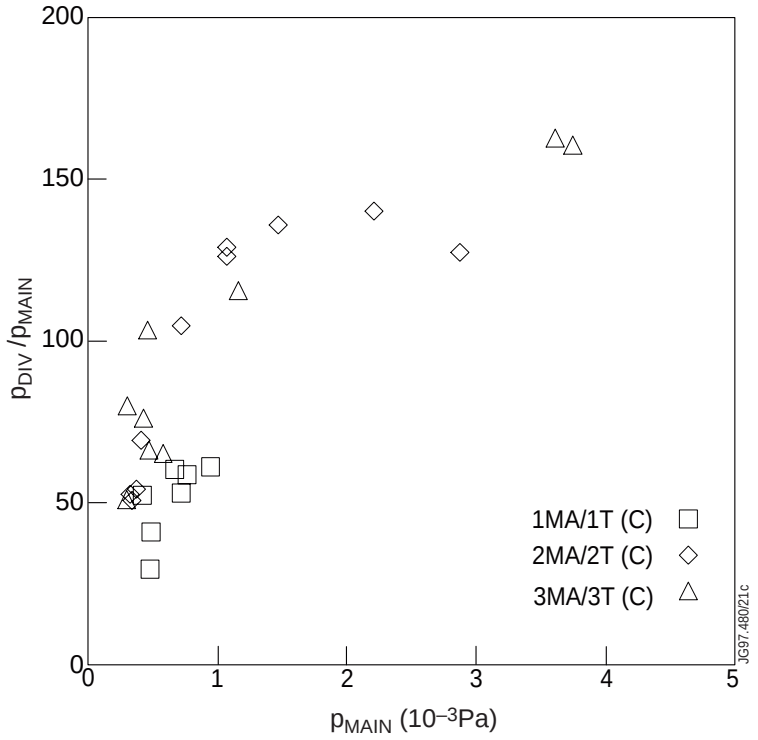

Figure 21. The main chamber pressure is shown here as a function of the compression ratio p_{DIV}/p_{MAIN}. A characteristic of detached plasmas is the decoupling of p_{MAIN} from p_{DIV}, shown here as decreasing compression ratio (or p_{DIV}) with increased p_{MAIN} and associated with neutrals escaping from the divertor into the main chamber. The effect is here particularly evident for the 2MA/2T series of data.

In a few cases, however, the effects of density and neutral pressure can be distinguished. In low or medium density plasmas the neutral pressure in the sub-divertor region and in the main chamber are in general a strong function of the edge density, and in these conditions it is very difficult to decouple them. At high main plasma density, however, it is well known in JET that the plasma tends to detach, with the inner divertor detaching earlier than the outer divertor (Loarte et *al*. 1997). In this case, while the plasma density both in the core and near the separatrix

increase, the neutral pressure in the main chamber increases more rapidly than that in the divertor. This loss of neutral compression is due to the increased neutral flux from the divertor to the main chamber, and related to the formation of MARFEs in the X-point region (Loarte et al. 1997). Under these circumstances, the influence of density and neutral pressure on the H-mode power threshold can be distinguished. This is evident in Fig.21, where the main chamber pressure p_{MAIN} is plotted for all three data series as a function of the compression ratio p_{DIV}/p_{MAIN}, and in Fig.22 for the 3MA/3T series in particular. At high values of the compression ratio the midplane pressure continues to increase, while the divertor pressure decreases. The discharges that show this anomalous behaviour are those in the high density regime, which deviate from the global linear (or quasi-linear) density scaling, namely #33446, 33447, 33450 (2MA/2T), 33460 and 33462 (3MA/3T). Section 3.4 showed in detail that these discharges are either partially detached, exhibit divertor oscillations, or both, contributing to the cooling of the plasma edge and loss of neutral compression, which in turn prevents the H-mode transition.

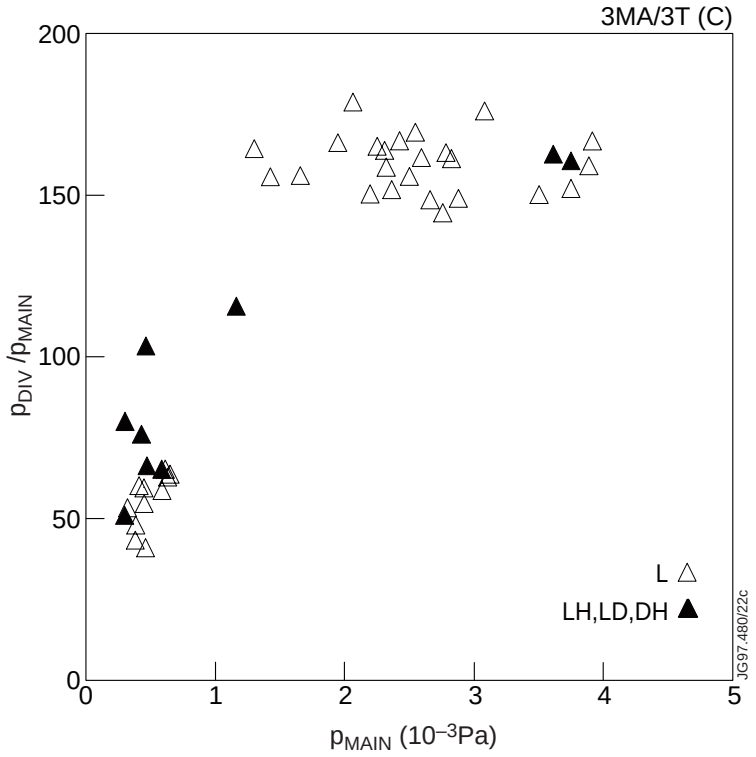

Figure 22. Same as in Fig.21, but only for the L-mode and L-H pre-transition data at 3MA/3T: the combination of L and L-H data-points also suggests that a turning point exists for the compression ratio, at which p_{MAIN} starts to increase more rapidly than p_{DIV}.

If these anomalous high density discharges are temporarily discarded from the analysis, those remaining should provide a relationship between edge density and neutral pressure both in the divertor and in the main chamber. This relationship is shown graphically in Fig.23, where

p_{DIV} (Fig.23a) and p_{MAIN} (Fig.23b) are plotted as a function of edge density. Qualitatively, Fig.23 shows that the density dependence is roughly quadratic, while the magnetic field dependence weakens with increasing B_t. Regression analysis quantifies the scaling:

$$p_{DIV} = (0.03 \pm 0.01) \times \bar{n}_{ea}^{(2.75 \pm 0.53)} \times B_t^{(-1.28 \pm 0.31)} \quad \text{(Pa)} . \tag{11}$$

$$p_{MAIN} = (0.37 \pm 0.05) \times \bar{n}_{ea}^{(1.60 \pm 0.19)} \times B_t^{(-0.64 \pm 0.14)} \quad (10^{-3}\ \text{Pa}) . \tag{12}$$

The dependence of p_{DIV} on the edge density is well documented (Ehrenberg et *al*. 1995) and is consistent with Eq.(11) and with a simple estimate for high recycling divertors (Loarte 1997). However this is the first time on JET that a scaling with the toroidal field has been observed. The dependence of p_{MAIN} on B_t could be due to as yet unsolved calibration problems. It is in fact known that changes in the current flowing in the shaping coils may influence the penning gauges, but so far it is not known to what degree the pressure measurements are affected (Andrew 1996). The fact that $P_{MAIN} \propto B_t^{-0.6}$, a relatively weak scaling, seems to point towards an instrumental rather than physical explanation.

The dependence of p_{DIV} on B_t is more difficult to explain. Measurements of the sensitivity of the ionisation gauges to changes in the toroidal field from 1T to 5T indicate that their calibration remains unchanged within less than 20% (Haas, Bosch and de Kock 1996). An independent measurement of the neutral flux estimated from the $D\alpha$ photon flux along the outer vertical line of sight is available from the visible spectrometer. From these data the same trend of Fig.23a emerges, quantified by the expression,

$$F_{MAIN} = (1.35 \pm 0.25) \times \bar{n}_{ea}^{(1.76 \pm 0.29)} \times B_t^{(-0.92 \pm 0.18)} \quad (10^{20}\ \text{particles}) . \tag{13}$$

This result rules out any errors in the calibration of the ionisation gauges. Using a "two-point,, model of the scrape-off layer (Keilhacker et *al*. 1982) the ion flux at the divertor can be obtained. Under non-detached conditions such ion flux is proportional to the divertor pressure. The derived scaling is,

$$p_{div}^0 \propto \frac{R^{4/7} a^{4/7}}{q^{6/7}} \times n_{sep}^2 \times \frac{\Delta^{10/7}}{P_{SOL}^{3/7}} , \tag{14}$$

where n_{sep} is the density at the separatrix, Δ is the SOL width and P_{SOL} is the power at the separatrix (P_{SOL}=P_{NET} in this case). From the experiment $P_{NET} \propto B_t$, but assumptions must be made about the dependencies of Δ. If $\Delta=\Delta(q)$ is assumed, then from Eq.(14) it follows that $p_{div}^0 \propto n_{sep}^2 / B_t^{3/7}$. On the other hand this scaling of the neutral pressure depends on the assumption used to describe the perpendicular transport in the SOL. Since the threshold database is formed mostly by pre-transition L-mode points, it would be reasonable to assume that core and edge transport are those characteristic of near L-mode conditions, i.e. Bohm-like. If the same transport is assumed to be valid also in the SOL, then $P_{DIV} \propto \bar{n}_{ea}^3 / B_t^2$, which is too strong if compared with Eq.(11). If instead Eq.(11) is assumed to be valid, from Eq.(14) and the linear scaling of P_{NET} with B_t it follows that $\chi_\perp \approx B_t^{14/63} / n_{sep}^{10/9}$, which implies an Alcator type of transport (Parker

1985). Clearly at this stage it is not possible to draw any firm conclusions from these data only, and a more detailed analysis is needed to establish the transport coefficients in the SOL just prior to the H-mode transition.

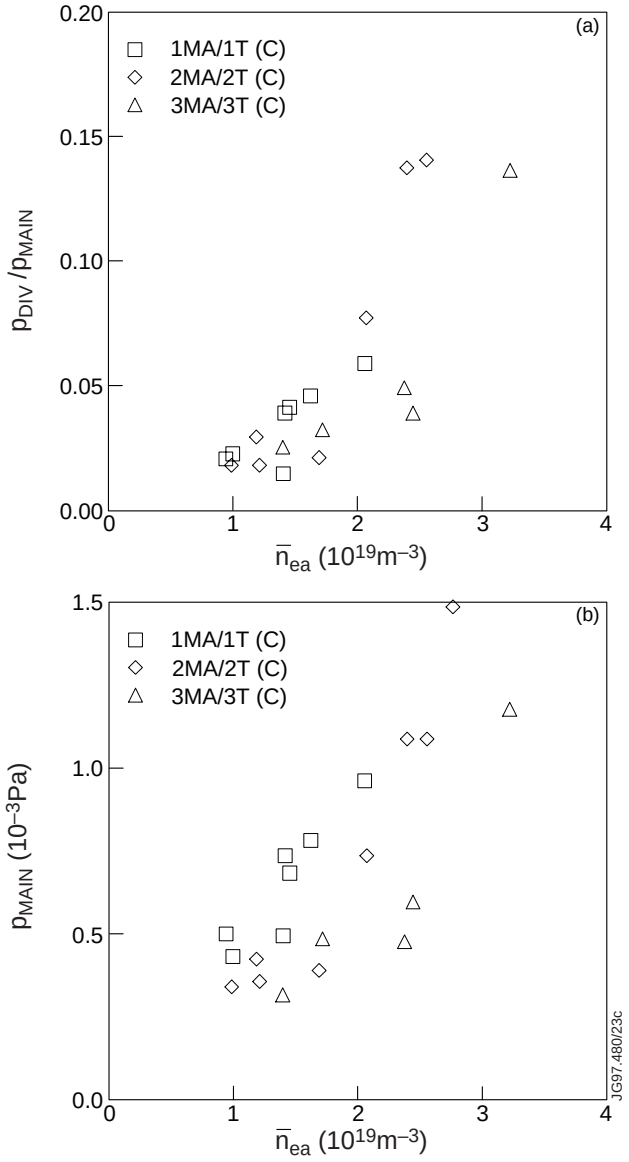

Figure 23. p_{DIV} (Fig.23a) and p_{MAIN} (Fig.23b) for the discharges of the database that are not detached shows a well known roughly quadratic scaling with the edge density $\overline{n}_{ea}$. More uncertain is the B_t dependence, which could be due to unknown influence of the magnetic field or coil currents on the gauges.

While the magnetic field dependence of the pressure measurements is too uncertain to draw firm conclusions (especially in the case of p_{MAIN}), in the case of a fixed magnetic field Eqs.(11-12) can help to describe the evolution of the H-mode power threshold with increasing density. As long as the density remains within the bounds of normal operating values for JET ($\overline{n}_e < 5\times10^{19}$ m^{-3}), any increase in density corresponds a roughly linear increase in the threshold power, and a

roughly quadratic increase in the neutral pressure in the divertor, while $\overline{n}_{ea} \propto p^{1.5}_{MAIN}$. Density and neutral pressure are in this case closely coupled together, and it is not possible to establish which of the two influence the threshold power. However when the density is further increased ($\overline{n}_e > 5\times10^{19}$ m^{-3}) by gas puffing and NBI fuelling, there is detachment of the inner divertor leg and, in some extreme cases, a MARFE instability in the X-point region. As a consequence neutrals escape from the divertor into the main chamber, thus affecting the edge of the plasma. Power in excess of that normally required for the L-H transition is needed to overcome the combination of partial detachment, divertor instability and abnormally high neutral pressure, all of which contribute to cool the plasma edge and keep T_{ea} below the critical value necessary for the H-mode transition.

Thus from the analysis of these data it can be concluded that, if very high density H-mode regimes are required, gas puffing (with the additional fuelling provided by NBI) is not the most effective way to achieve them. Excessive edge fuelling requires more power to compensate for edge cooling. However this problem could be overcome by using high speed pellets, which fuel efficiently in the plasma centre without cooling the edge.

4. SUMMARY AND CONCLUSIONS

A series of experiments devoted to investigate the dependence of the H-mode power threshold on the plasma density were carried out on JET during the 1994/95 Experimental Campaign with the MkI Pumped Divertor. The experiments were carried out in an ITER-like configuration while keeping $q_{95} \cong 3$ at the L-H transition. The discharges thus obtained are part of the 1994/95 JET contribution to the multi-machine Threshold Database used to extrapolate the H-mode power threshold to ITER.

The experiments used both CFC and beryllium as divertor target materials. In both cases the power threshold remains essentially the same, allowing us to conclude that the choice of different low Z target materials for the divertor target in ITER should not influence the threshold power.

Together with measurements of the electron density both in the plasma centre and at the edge, data have been obtained of the edge electron and ion temperatures, as well as the neutral pressure in the main chamber and in the sub-divertor region. All these measurements combine to give a clear picture of the evolution of P_{THRES} when the density is increased well above the normal operational values for JET.

At low to medium density ($\overline{n}_e = 1\text{-}5\times10^{19}$ m^{-3}) the power threshold follows the well established scaling expression with a linear or almost linear ($\overline{n}_e^{0.75}$) scaling with the central line averaged density and linear scaling with the toroidal field B_t. Both density scalings, $P_{LOSS} \propto \overline{n}_e$ and $P_{LOSS} \propto \overline{n}_e^{0.75}$ give reasonable fits to the data, due to the difficulty in reducing the scatter in the data that is intrinsic to these experiments. At the same time the neutral pressure in the main

chamber and in the divertor scale with the edge density following well known laws. The dependence of the neutral pressure on the toroidal field is however uncertain: while for p_{DIV} there could be some justification for the observed behaviour based on perpendicular transport in the SOL, the pressure in the main chamber is suspected to be influenced by currents in the shaping coils, which complicates the interpretation of the B_t scaling.

Measurements of the edge electron temperature just prior to the H-mode transition show that a minimum edge T_e is necessary for the L-H transition to occur. Such critical temperature is weakly dependent on the edge density, and strongly dependent on the toroidal field, $T_{crit} \propto B_t^2$.

The power threshold, expressed as the net power flowing through the separatrix, has also been related to edge quantities. A scaling expression roughly linear with $\overline{n}_{ea}$ has been shown to be valid for P_{NET} ($\propto \overline{n}_{ea}^{0.95}$).

At densities above 5×10^{19} m^{-3} deviations from the linear or quasi-linear scaling expressions are evident when considering both the centre and edge densities. The increased power necessary for the H-mode transition under these conditions has been associated with the presence of partial detachment and/or divertor oscillations, both induced by the strong gas puffing necessary to reach such high densities. The Langmuir probes in the divertor target tiles show detachment at the inner divertor leg for all the discharges deviating from the linear density scaling. For these discharges decoupling of the neutral pressure at the midplane from that at the divertor is observed, due to leakage of neutrals from the divertor into the main chamber commonly associated with detachment. The neutrals escaping from the divertor due to detachment act to cool the plasma edge and prevent access to the H-mode regime. If a partially detached plasma is considered for ITER, then the advantages of reduced power load on the divertor target tiles must be weighed against the increased power demand necessary to obtain the H-mode, and the rather poor confinement that such an H-mode would probably have. If very high densities are needed, then deeply penetrating pellets may be the only way to fuel the plasma centre without disturbing the edge.

In the high density regime the edge electron temperature behaves consistently with the scaling described by Eq.(8). Due to the excessive edge cooling, T_{ea} reaches the critical temperature necessary for the L-H transition only when the power is increased sufficiently to compensate, and the plasma remains in H-mode only as long as $T_{ea} > T_{crit}$. These observations lead us to draw two main conclusions regarding the relationship between edge temperature and H-mode transition. Firstly, the existence of the minimum critical temperature is a necessary condition for the L-H transition, but as yet there are no indications on JET that this condition is also sufficient. Secondly, as far as the edge parameters are concerned, there is no reason to believe that there is any hysteresis effect for the H-L transition, and that L-H/H-L transitions are in this respect symmetric.

REFERENCES

Andrew P (1996), private communication.

ASDEX Team (1989), Nucl. Fusion **29**, 1959.

Carlstrom TN et *al.* (1996), Plasma Phys. and Controlled Fusion **38(8)**, 1231.

Erckmann V et *al.* (1993), Phys. Rev. Lett. **70**, 2086.

Groebner RJ et *al*. (1996), Proc. 16th IAEA Fusion Energy Conference, Montreal (Canada), IAEA-F1-CN-64/AP2-10.

Haas G, Bosch HS and de Kock L. (1996), in *Diagnostics for Experimental Thermonuclear Reactors*, ed. P Stott et al., Plenum Press, NY, pp.571.

JFT-2M Team (1991), Proc. 3rd H-mode Workshop **1**,141.

Kaufman M et *a*. (1996), Proc. 16th IAEA Fusion Energy Conference, Montreal (Canada), IAEA-F1-CN-64/1-5.

Keilhacker M et *al*. (1982), Physica Scripta **T2/2**, 443.

Lackner K et *al.* (1994), Plasma Phys. Controlled Fusion **36B(12)**, 79.

Loarte A et *al*. (1997), JET pre-print JET-P(97)03, submitted for publication in Nucl. Fusion.

Monk RD et *al*. (1995), Proc. 22nd EPS Conference on Controlled Fusion and Plasma Physics, Bournemouth (UK), Vol. 19C, III-293.

Monk RD (1996), Ph.D. Thesis, University of London.

Nardone C et *al.* (1991), Proc. 18th EPS Conference on Controlled Fusion and Plasma Physics, Berlin, **15C**, I-377.

Parker RR (1985), Nucl. Fusion **25**, 1127.

Righi E et *al.* (1995), Proc. 22nd EPS Conference on Controlled Fusion and Plasma Physics, Bournemouth (UK), .**19C**, II-73.

Righi E et *al*. (1997), Proc. 24th EPS Conference on Controlled Fusion and Plasma Physics, Berchtesgaden (Germany).

Ryter F. et *al.* (1991), Proc. 19th EPS Conference on Controlled Fusion and Plasma Physics, Innsbruck (Austria), **16C**, I-195.

Ryter F et *al.* (1992), Proc. 20th EPS Conference on Controlled Fusion and Plasma Physics, Lisbon, **17C**, I-15.

Ryter F et *al.* (1996), Nucl. Fusion **36**, 1217.

Saibene G et *al.* (1995), Proc. 22nd EPS Conference on Controlled Fusion and Plasma Physics, Bournemouth (UK), .**19C**, II-121.

Saibene G et *al*. (1997), J. Nucl. Mat. **241-243**, P. 476.

Start DFH et *al.* (1994), Proc. 21st EPS Conference on Controlled Fusion and Plasma Physics, Montpellier, **18B**, I-314.

Snipes J et *al*. (1996), Proc. 16th IAEA Fusion Energy Conference, Montreal (Canada), IAEA-CN-64/AP2-11.

Takizuka T et *al*. (1996), Proc. 16th IAEA Fusion Energy Conference, Montreal (Canada), IAEA-CN-64/F-5.

Wagner F et *al.* (1982), Phys. Rev. Lett. **49**, 1408.

Ward D et *al.* (1991), Proc. 18th EPS Conference on Controlled Fusion and Plasma Physics, Berlin, **15C**, I-353.